frontiers | Frontiers in Physics

TYPE Brief Research Report
PUBLISHED 12 October 2022
DOI 10.3389/fphy.2022.992239

OPEN ACCESS

EDITED BY
Ramon Planet,
University of Barcelona, Spain

REVIEWED BY
Rushi Kumar B,
VIT University, India
Prasenjit Das,
Indian Institute of Science Education and Research Mohali, India

*CORRESPONDENCE
Kuniyasu Saitoh,
k.saitoh@cc.kyoto-su.ac.jp

SPECIALTY SECTION
This article was submitted to Soft Matter Physics,
a section of the journal
Frontiers in Physics

RECEIVED 12 July 2022
ACCEPTED 21 September 2022
PUBLISHED 12 October 2022

CITATION
Saitoh K and Kawasaki T (2022), Shear-induced diffusion and dynamic heterogeneities in dense granular flows. *Front. Phys.* 10:992239.
doi: 10.3389/fphy.2022.992239

Shear-induced diffusion and dynamic heterogeneities in dense granular flows

Kuniyasu Saitoh[1]* and Takeshi Kawasaki[2]

[1]Department of Physics, Faculty of Science, Kyoto Sangyo University, Kyoto, Japan, [2]Department of Physics, Nagoya University, Nagoya, Japan

We study two-dimensional dense granular flows by molecular dynamics simulations. We quantify shear-induced diffusion of granular particles by the transverse component of particle displacements. In long time scales, the transverse displacements are described as normal diffusion and obey Gaussian distributions, where time correlations of particle velocities entirely vanish. In short time scales, the transverse displacements are strongly non-Gaussian if the system is dense and sheared quasistatically though memory effects on the particle velocities are further suppressed. We also analyze spatio-temporal structures of the transverse displacements by self-intermediate scattering functions and dynamic susceptibilities. We find that the relation between the maximum intensity and characteristic time scale for dynamic heterogeneities is dependent on the models of contact damping (which exhibit different rheological properties such as the Newtonian fluids' behavior and shear thickening). In addition, the diffusion coefficient over the shear rate is linear (sub-linear) in the maximum of dynamic susceptibility if the damping force is not restricted (restricted) to the normal direction between the particles in contact.

KEYWORDS

diffusion, dynamic heterogeneities, granular flow, jamming transition, rheology

1 Introduction

Flows of granular materials are of great importance to engineering technology [1, 2] and a better understanding of their transport phenomena is crucial to many industrial processes such as *mixing* and *segregation* [3]. Because constituent grains are macroscopic in size, e.g., are typically from few μm to mm in diameter [4], thermal fluctuations do not play a role in flows and transport phenomena of granular materials. This means that granular flows are induced only by external forces and "mechanically driven" particle motions have extensively been studied by experiments [5–12] and numerical simulations [13–19]. It now seems to be a common consensus that collective motions of granular particles are more pronounced as the system approaches the *jamming transition* [20].

In recent years, diffusion of the particles under shear, i.e. *shear-induced diffusion*, has widely been investigated by experiments [21–25] and molecular dynamics (MD) simulations [26–31]. From a scaling argument, the shear-induced diffusion coefficient

scales as $D \sim d_0^2\dot{\gamma}$ with the particle diameter d_0 and externally imposed shear rate $\dot{\gamma}$ [21–23]. The scaling argument implies that the diffusion coefficient is proportional to the shear rate. However, a crossover from $D \propto \dot{\gamma}$ to $\dot{\gamma}^{0.8}$ (with increasing $\dot{\gamma}$) was observed in MD simulations of two- and three-dimensional particles [16, 26]. These results agree with laboratory experiments of colloidal glasses under shear [24] and suggest that the shear-induced diffusion does not depend on spatial dimensions. Another crossover from $D \propto \dot{\gamma}$ to $\dot{\gamma}^{1/2}$ was also found in a model of amorphous solids [29]. In addition, sub-linear scaling, $D \propto \dot{\gamma}^{q_D}$, was examined near the jamming transition density ϕ_J, where the exponent varies as $q_D = 1$ ($\phi < \phi_J$), 0.78 ($\phi \simeq \phi_J$), and 0.68 ($\phi > \phi_J$) with the increase of particle packing fraction ϕ [27].

The collective motions of the particles enhance self-diffusion and thus the scaling argument was revised as $D \sim d_0\xi\dot{\gamma}$ with a typical size of collective motions, ξ [28]. The typical size can be extracted, e.g. from a spatial correlation function of particle velocities, and it has been suggested that $\xi \sim \dot{\gamma}^{-0.23}$ near jamming ($\phi \simeq \phi_J$) [16] and $\xi \sim \dot{\gamma}^{-1/2}$ above jamming ($\phi > \phi_J$) [28, 29]. If the system is below jamming ($\phi < \phi_J$), critical divergence of the size was found as $\xi \sim |\Delta\phi|^{-0.6}$ in overdamped MD simulations [20], where $\Delta\phi \equiv \phi - \phi_J$ is the proximity to jamming. However, $\xi \sim |\Delta\phi|^{-1}$ was reported in quasi-static simulations [32].

In addition to the shear-induced diffusion, analogies with *dynamic heterogeneities* [33, 34] have also been made by experiments [9, 10] and numerical simulations [15–17]. Associating the mechanical driving with thermal fluctuations, the physicists have analyzed heterogeneous nature of particle motions both in space and time. Then, a link between the shear-induced diffusion and dynamic heterogeneities was suggested as $D \sim \chi_s^*\dot{\gamma}$ by the elastoplastic model in two-dimension (not in three-dimension) [35], where χ_s^* represents the maximum intensity of dynamic heterogeneities. Results in prior works, however, are controversial, e.g. the maximum intensity scales as $\chi_s^* \sim |\Delta\phi|^{-1.8}$ for $\phi < \phi_J$ and $\chi_s^* \sim$ const. for $\phi > \phi_J$ in quasi-static simulations [17], while $\chi_s^* \sim |\Delta\phi|^{-1.2}\dot{\gamma}^{-0.3}$ was suggested for both below and above jamming by experiments [10]. Moreover, the scaling, $D \sim \chi_s^*\dot{\gamma}$, has not yet been tested by MD simulations of sheared granular materials. Interestingly, particle motions in oscillatory sheared granular materials [6], air-fluidized bed [7], and horizontally vibrated granular media [36] have similarities to glass forming liquids [33, 34], where both length and time scales for dynamic heterogeneities diverge at the jamming transition density.

In this paper, we study the shear-induced diffusion and dynamic heterogeneities in dense granular flows by MD simulations. We investigate wide ranges of control parameters, i.e. the packing fraction of the particles ϕ and shear rate $\dot{\gamma}$, to examine the scaling relation, $D \sim \chi_s^*\dot{\gamma}$, both below and above jamming, and in both quasi-static and fast flow regimes. In the following sections, we introduce our numerical method in Section 2 and show our results in Section 3. Then, we discuss our results in Section 4 and conclude our findings in Section 5.

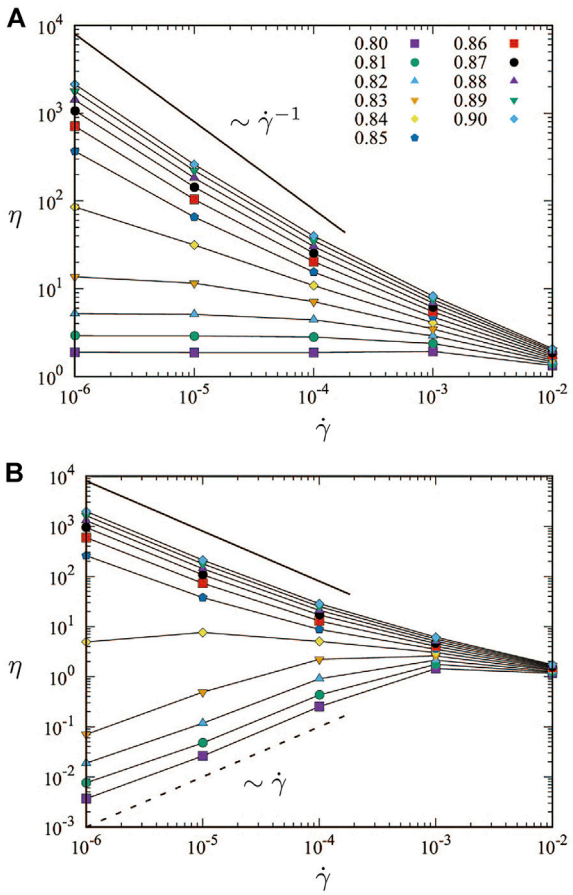

FIGURE 1
Double logarithmic plots of the shear viscosity η and shear rate $\dot{\gamma}$, where the models **(A)** A and **(B)** B are used for the damping force, $\boldsymbol{f}_{ij}^{\mathrm{d}}$. The packing fraction of the particles ϕ increases as listed in the legend of **(A)**. The solid lines indicate shear thinning, $\eta \sim \dot{\gamma}^{-1}$, whereas the dashed line in **(B)** represents the Bagnold scaling (shear thickening), $\eta \sim \dot{\gamma}$.

2 Method

We study dense granular flows in two dimensions by MD simulations. To avoid crystallization of the system, we randomly distribute a 50 : 50 binary mixture of $N = 2048$ particles in a $L \times L$ square periodic box. Different kinds of particles have the same mass m and different diameters, d_S and $d_L = 1.4d_S$ [20, 37]. Repulsive force between the particles, i and j, in contact is modeled as elastic force, $\boldsymbol{f}_{ij}^{\mathrm{e}} = k_{\mathrm{e}}l_{ij}\boldsymbol{n}_{ij}$, where k_{e} is a spring constant and $\boldsymbol{n}_{ij} \equiv \boldsymbol{r}_{ij}/|\boldsymbol{r}_{ij}|$ with the relative position between the particles, $\boldsymbol{r}_{ij}$, is the normal unit vector. Here, $l_{ij} \equiv R_i + R_j - |\boldsymbol{r}_{ij}| > 0$ represents an overlap between the particles, where R_i (R_j) is the

radius of $i(j)$-th particle. Damping force is also introduced between the particles in contact as $\boldsymbol{f}_{ij}^{\mathrm{d}}$, where we examine two different force laws according to Ref. [38]: (i) The damping force is given by $\boldsymbol{f}_{ij}^{\mathrm{d}} = -\eta_{\mathrm{d}}\boldsymbol{v}_{ij}$, where η_{d} is a damping constant and $\boldsymbol{v}_{ij}$ is the relative velocity between the particles. We refer to this model as *model A*. (ii) The damping force is restricted to the normal direction as $\boldsymbol{f}_{ij}^{\mathrm{d}} = -\eta_{\mathrm{d}}(\boldsymbol{v}_{ij}\cdot\boldsymbol{n}_{ij})\boldsymbol{n}_{ij}$, which is often used for a model of "frictionless granular particles" [39]. We refer to this model as *model B*. In both the models A and B, we choose the spring and damping constants as the normal restitution coefficient is given by $e = \exp(-\pi/\sqrt{2mk_{\mathrm{e}}/\eta_{\mathrm{d}}^2 - 1}) \simeq 0.8$ [40].

We simulate simple shear flows of the system under the Lees-Edwards boundary condition. In each time step, every particle position $\boldsymbol{r}_i = (x_i, y_i)$ is replaced with $(x_i + \Delta\gamma y_i, y_i)$ $(i = 1, \ldots, N)$ and then equations of motion, $m\ddot{\boldsymbol{r}}_i = \sum_j(\boldsymbol{f}_{ij}^{\mathrm{e}} + \boldsymbol{f}_{ij}^{\mathrm{d}})$, are numerically integrated with a small time increment, $\Delta t = 0.1t_0$. Here, $t_0 \equiv \eta_{\mathrm{d}}/k_{\mathrm{e}}$ is a time unit and $\Delta\gamma$ is a strain increment such that the shear rate is defined as $\dot{\gamma} = \Delta\gamma/\Delta t$. In the following, we analyze the data in a steady state (where the amount of shear strain exceeds unity) and scale every mass, time, and length by m, t_0, and the mean particle diameter, $d_0 \equiv (d_S + d_L)/2$, respectively.

3 Results

In this section, we show our numerical results of shear-induced diffusion and dynamic heterogeneities in dense granular flows. We clarify the role of packing fraction of the particles ϕ and shear rate $\dot{\gamma}$. In addition, we examine how rheological properties of the particles affect our results. Figure 1 displays our numerical results of shear viscosity $\eta = \sigma/\dot{\gamma}$, where σ is shear stress. The shear stress is calculated as $\sigma = -L^{-2}\sum_{i<j} f_{ijx}^{\mathrm{e}} r_{ijy}$ with the x- and y-components of the elastic force and relative position, f_{ijx}^{e} and r_{ijy}, respectively, and is averaged over 10^3 different configurations of the particles in a steady state. In this figure, we used the models (A) A and (B) B for the contact damping, $\boldsymbol{f}_{ij}^{\mathrm{d}}$, and changed the packing fraction from $\phi = 0.80$ to 0.90 (symbols). If the packing fraction is much smaller than the jamming transition density, $\phi_J \simeq 0.8433$ [20], the model A exhibits the Newtonian fluids' behavior, i.e. η ~const., for sufficiently small shear rates. In contrast, the model B shows the Bagnold scaling, $\sigma \sim \dot{\gamma}^2$, i.e. $\eta \sim \dot{\gamma}$ (dashed line). If the packing fraction is larger than ϕ_J, both the models exhibit the rate-independent yield stress, $\sigma = \sigma_Y$, so that one observes shear thinning as $\eta \sim \dot{\gamma}^{-1}$ (solid lines). See also the Supplementary Material (SM) [41] for our numerical results of *flow curves*, i.e., σ vs. $\dot{\gamma}$. In the following analyses, we explain how the difference between the models A and B influences the shear-induced diffusion and dynamic heterogeneities.

Since our system is homogeneously sheared along the x-direction, we analyze fluctuating transverse motions of the particles along the y-direction. We introduce a transverse displacement of the particle i $(= 1, \ldots, N)$ as the time integral,

$$\delta y_i(\tau) = \int_{t_a}^{t_a+\tau} v_{iy}(t)dt \ , \tag{1}$$

where τ is a time interval and $v_{iy}(t)$ is the y-component of particle velocity [42]. Note that the initial time t_a can arbitrary be chosen during a steady state.

In the following, we associate the fluctuating transverse motions of the particles (Eq. 1) with thermally activated molecular motions in glasses [33]. We show how the shear-induced diffusion is controlled by the parameters, ϕ and $\dot{\gamma}$ (Section 3.1), and analyze dynamic heterogeneities (Section 3.2). Then, we examine the relation between the maximum intensity and characteristic time scale for dynamic heterogeneities (Section 3.3) and discuss the link between the shear-induced diffusion and dynamic heterogeneities (Section 3.4).

3.1 Shear-induced diffusion

We quantify shear-induced diffusion of the particles by the transverse component of *mean squared displacement* (MSD) [42],

$$\Delta^2(\tau) = \langle \frac{1}{N}\sum_{i=1}^{N}\delta y_i(\tau)^2 \rangle_{t_a} \ , \tag{2}$$

where the ensemble average $\langle \ldots \rangle_{t_a}$ is taken over different choices of the initial time t_a (see Eq. 1). Figures 2A,B display the MSDs with different values of the control parameters, (A) ϕ and (B) $\dot{\gamma}$, where the scaled shear rate and packing fraction are fixed to (A) $\dot{\gamma}t_0 = 10^{-4}$ and (B) $\phi = 0.84$, respectively. The horizontal axes are the time interval τ scaled by the shear rate $\dot{\gamma}$, i.e. the shear strain applied to the system for the duration, $\gamma \equiv \dot{\gamma}\tau$. In this figure, we used the model A for the damping force (see SM [41] for the results of model B, where we confirm that the results are qualitatively the same). As can be seen, every MSD exhibits a cross-over from super-diffusion to normal diffusion, $\Delta^2(\tau) \sim \dot{\gamma}\tau$ (dashed lines), around a cross-over strain, $\gamma = \gamma_c < 1$ [17]. The MSDs monotonously increase with the increase of packing fraction ϕ (Figure 2A), whereas they decrease with the increase of shear rate $\dot{\gamma}$ (Figure 2B). In simple shear flows, transverse motions of the particles are induced by contacts. The denser the system is, the more likely the particles make contacts. In addition, the particles can travel long distance during a certain strain interval if the shear rate is small. Therefore, transverse motions of the particles are most enhanced in quasi-static flows of dense systems [19]. Different from glass forming liquids [33], any plateaus are not observed in the MSDs. This means that neither *caging* nor *sub-diffusion* of the particles exists in our system [15–17]. Note that the MSDs defined by *non-affine displacements* show qualitatively the same results (data are not shown).

We also analyze time correlations of transverse motions by the *velocity auto-correlation function* (VACF),

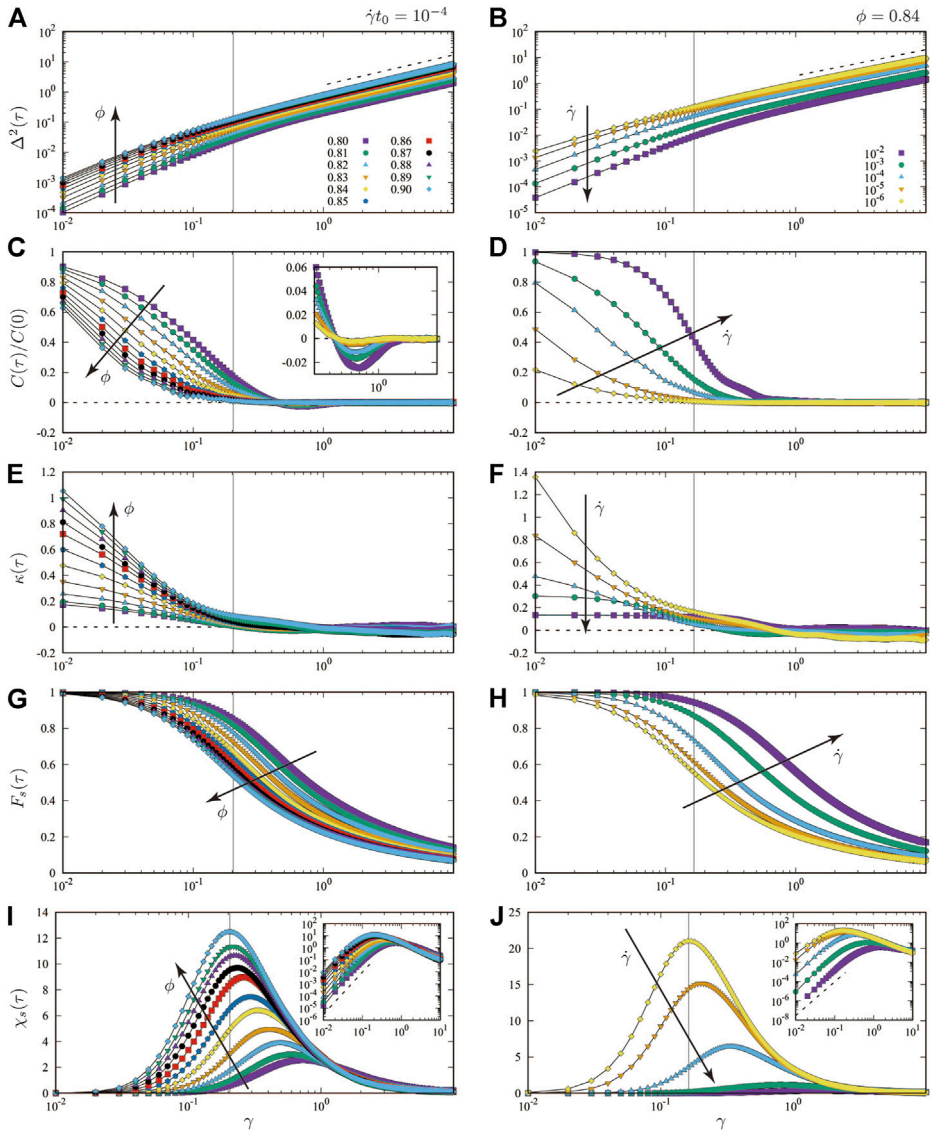

FIGURE 2
The MSD $\Delta^2(\tau)$ (**(A)** and **(B)**), normalized VACF $C(\tau)/C(0)$ (**(C)** and **(D)**), non-Gaussian parameter $\kappa(\tau)$ (**(E)** and **(F)**), self-intermediate scattering function $F_s(\tau)$ (**(G)** and **(H)**), and dynamic susceptibility $\chi_s(\tau)$ (**(I)** and **(J)**) as functions of the shear strain $\gamma = \dot{\gamma}\tau$, where we used the model A for the damping force (see the SM [41] for the results of model B). In **(A)**, **(C)**, **(E)**, **(G)**, and **(I)**, we increase the packing fraction of the particles ϕ as listed in the legend of **(A)**, where the scaled shear rate is given by $\dot{\gamma}t_0 = 10^{-4}$. In **(B)**, **(D)**, **(F)**, **(H)**, and **(J)**, we decrease the scaled shear rate $\dot{\gamma}t_0$ as listed in the legend of **(B)**, where the packing fraction is fixed to $\phi = 0.84$. The dashed lines in **(A)** and **(B)** indicate the normal diffusion, $\Delta^2 \sim \dot{\gamma}\tau$, while those in **(C)**–**(F)** represent zero. The inset to **(C)** is a zoom-in to the data for $\phi < \phi_J \simeq 0.8433$ and $\dot{\gamma}t_0 = 10^{-4}$. The insets to **(I)** and **(J)** are double logarithmic plots, where the dashed lines indicate the power-law behavior (with the slope 3.5). The vertical solid lines represent the peak positions of the dynamic susceptibility, i.e. $\gamma^* = \dot{\gamma}\tau^*$, for $\phi = 0.90$ (**(A)**, **(C)**, **(E)**, **(G)**, and **(I)**) and $\dot{\gamma}t_0 = 10^{-6}$ (**(B)**, **(D)**, **(F)**, **(H)**, and **(J)**). Note that all the results have been averaged over 10^2 samples.

$$C(\tau) = \langle \frac{1}{N} \sum_{i=1}^{N} v_{iy}(t_a + \tau) v_{iy}(t_a) \rangle_{t_a} . \quad (3)$$

Figures 2C,D show the normalized VACFs, $C(\tau)/C(0)$, where ϕ and $\dot{\gamma}$ vary as in Figures 2A,B, respectively. As can be seen, every VACF decays to zero if the shear strain exceeds the cross-over strain, $\gamma > \gamma_c$. Therefore, transverse velocities of the particles completely lose their memory when the system exhibits the normal diffusion (dashed lines in Figures 2A,B). If the packing fraction is small enough, i.e. $\phi < \phi_J$, one observes that the VACFs are lowered to negative values and then converge to zero (see the inset to (C)), indicating *backscattering* of the particles [43]. Note that the backscattering effects are weakened if we use the model B for the damping force (see

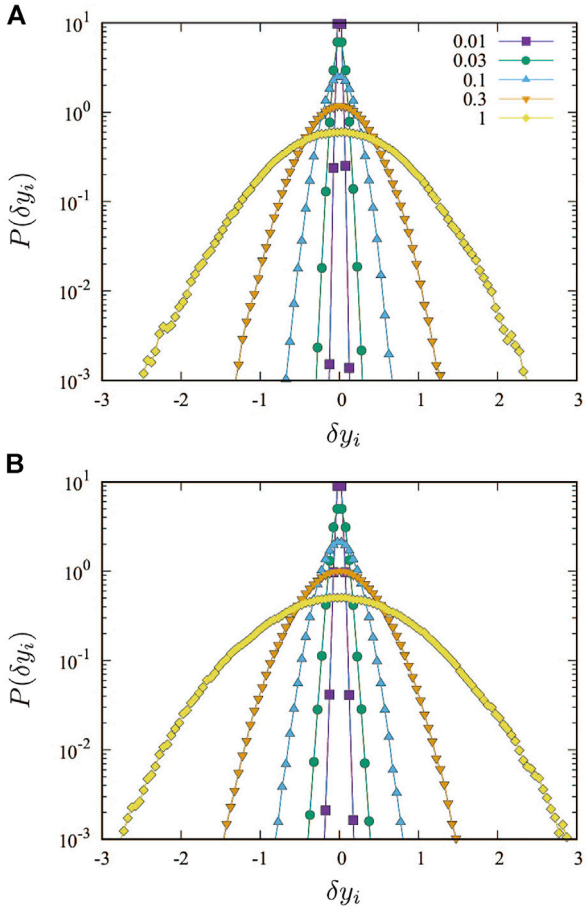

FIGURE 3
Semi-logarithmic plots of the PDFs of transverse displacements $\delta y_i(\tau)$ ($i = 1, \ldots, N$), where the models **(A)** A and **(B)** B are used for the damping force. The shear strain increases from $\gamma = \dot{\gamma}\tau = 10^{-2}$ to 1 as listed in the legend of **(A)**, where the control parameters are given by $\phi = 0.84$ and $\dot{\gamma}t_0 = 10^{-4}$.

SM [41]). In short time scales, $\gamma < \gamma_c$, the VACF decays faster if we increase ϕ (Figure 2C) or decrease $\dot{\gamma}$ (Figure 2D). Thus, the time correlations, as well as memory effects on transverse motions, are strongly suppressed in quasi-static flows of dense systems.

The probability distribution function (PDF) of particle displacements is associated with the *self-van Hove function* which is another important measure of diffusion [43]. Figure 3 shows our numerical results of the PDFs of transverse displacements, $P(\delta y_i(\tau))$, where the models (A) A and (B) B are used for the contact damping. In this figure, each PDF has been averaged over 10^2 samples. As can be seen, the PDFs are quite insensitive to the models and are symmetric around $\delta y_i(\tau) = 0$, indicating that the anisotropy is negligible in our systems [44].

The width (variance) of the PDF is equivalent to the MSD, while the shape of the PDF is characterized by the *non-Gaussian parameter*,

$$\kappa(\tau) = \frac{\langle N^{-1}\sum_{i=1}^{N}\delta y_i(\tau)^4\rangle_{t_a}}{\langle N^{-1}\sum_{i=1}^{N}\delta y_i(\tau)^2\rangle_{t_a}^2} - 3\ . \tag{4}$$

The non-Gaussian parameter is defined as the kurtosis subtracted by three, which quantifies how the PDF deviates from the normal distribution (where $\kappa(\tau) = 0$). Figures 2E,F display the time development of non-Gaussian parameters, $\kappa(\tau)$, where the control parameters change as in Figures 2A,B. In this figure, we used the model A for the damping force (see SM [41] for the results of model B). The non-Gaussian parameters converge to zero if the strain exceeds the cross-over strain, $\gamma > \gamma_c$, regardless of ϕ and $\dot{\gamma}$. This means that the transverse displacements obey Gaussian distributions and thus are uncorrelated in space when the shear-induced diffusion is described as the normal diffusion. When molecules in a glass escape from a cage, the self-van Hove function strongly deviates from the normal distribution [45] so that the non-Gaussian parameter exhibits a characteristic peak. In our system, the non-Gaussian parameters do not show peaks because the particles are not trapped by cages and do not undergo sub-diffusion. Nevertheless, in short time scales ($\gamma < \gamma_c$), the non-Gaussian parameter tends to be large for $\phi > \phi_J$ (Figure 2E) and $\dot{\gamma}t_0 \ll 1$ (Figure 2F), implying that "transverse velocities" in quasi-static flows of dense systems are strongly non-Gaussian and may be spatially correlated [19].

3.2 Dynamic heterogeneities

Next, we examine dynamic heterogeneities of transverse motions of the particles. To quantify the dynamics of single particles, we introduce the *self-intermediate scattering function* as $F_s(\tau) = \langle \hat{f}_s(\tau)\rangle_{t_a}$, where the function is defined as

$$\hat{f}_s(\tau) = \frac{1}{N}\sum_i \frac{\sin[k\delta y_i(\tau)]}{k\delta y_i(\tau)} \tag{5}$$

with the wave number, $k = 2\pi/d_0$. Figures 2G,H show the time development of self-intermediate scattering functions, $F_s(\tau)$, where the parameters, ϕ and $\dot{\gamma}$, vary as in Figures 2A,B, respectively (see SM [41] for the results of model B). In these figures, $F_s(\tau)$ monotonously decreases from one to zero and does not exhibit a plateau as we do not observe any plateaus in the MSDs. In addition, it becomes sufficiently small, $F_s(\tau) < 0.5$, when the shear-induced diffusion is described as the normal diffusion. This means that most of the transverse displacements are greater than the particle radius if $\gamma > \gamma_c$ (as can be seen in the data of MSDs). In short time scales ($\gamma < \gamma_c$), $F_s(\tau)$ decays faster if we increase ϕ (Figure 2G) or decrease $\dot{\gamma}$ (Figure 2H). Therefore, the magnitude of transverse displacements is most enhanced in quasi-static flows of dense systems [19].

To further investigate spatio-temporal heterogeneous structures of transverse motions, we calculate the *dynamic susceptibility* as the variance of the function $\hat{f}_s(\tau)$, i.e.

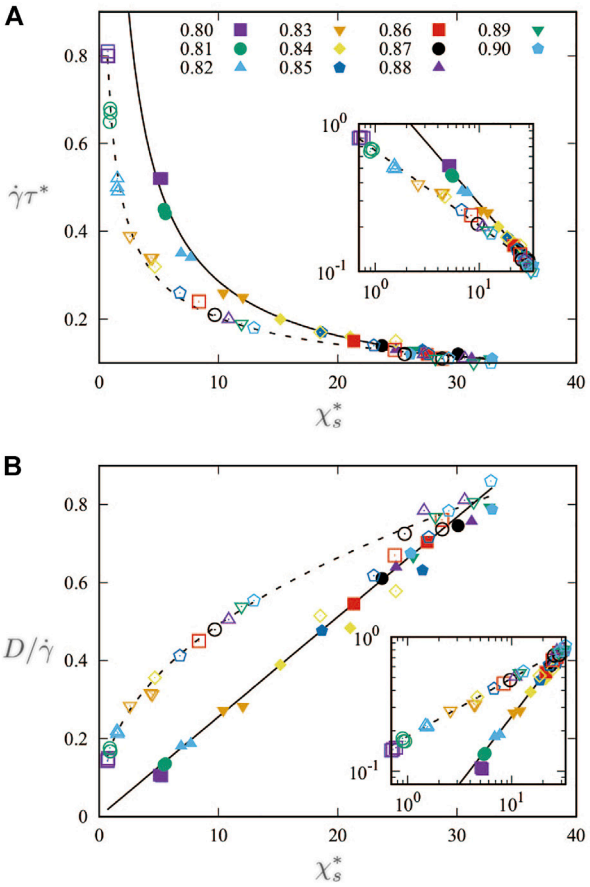

FIGURE 4
(A) The peak position of dynamic susceptibility, $\dot{\gamma}\tau^*$, and **(B)** diffusion coefficient over the shear rate, $D/\dot{\gamma}$, as functions of the maximum intensity of dynamic heterogeneities, χ_s^*, where the packing fraction ϕ increases as listed in the legend of **(A)**. The solid (open) symbols are the results of model A (B), where we only show the data in a quasi-static regime, $\dot{\gamma}t_0 \leq 10^{-5}$ (10^{-4}). In **(A)**, the solid (dashed) line is a power-law fit, $\dot{\gamma}\tau^* \sim \chi_s^{*-0.82}$ ($\chi_s^{*-0.51}$), to the data of model A (B). In **(B)**, the solid line is the linear scaling, $D/\dot{\gamma} \sim \chi_s^*$, for the results of model A, while the dashed line is a power-law fit, $D/\dot{\gamma} \sim \chi_s^{*0.43}$, to the data of model (B). The insets are double logarithmic plots.

$$\chi_s(\tau) = N\left\{\langle \hat{f}_s(\tau)^2\rangle - \langle \hat{f}_s(\tau)\rangle^2\right\}. \quad (6)$$

Figures 2I,J display the time development of dynamic susceptibilities, $\chi_s(\tau)$, where the control parameters change as in Figures 2A,B (see SM [41] for the results of model B). As in the case of glass forming liquids [34], $\chi_s(\tau)$ has a single peak at a characteristic time scale, τ^*. The height of the peak, $\chi_s^* \equiv \chi_s(\tau^*)$, representing the maximum intensity of the heterogeneities, grows with the increase of ϕ (Figure 2I) [17] and decrease of $\dot{\gamma}$ (Figure 2J). On the other hand, the peak position $\dot{\gamma}\tau^*$ decreases with increasing ϕ and decreasing $\dot{\gamma}$. This is in sharp contrast to the dynamic heterogeneities in glasses [34] and homogeneously driven granular materials [7], where *both* the peak height and position, χ_s^* and τ^*, increase when the systems approach the glass and jamming transitions. Note that the peak position $\dot{\gamma}\tau^*$ (vertical solid lines in Figure 2) is around (or less than) the cross-over strain γ_c. Moreover, we also find the power-law growth of dynamic susceptibility before the peak (dashed lines in the insets to (I) and (J)) as previously reported by experiments of two-dimensional granular materials under shear [6].

3.3 Dynamic criticality

In the case of glass forming liquids and homogeneously driven granular materials, both the peak height χ_s^* and position τ^* of dynamic susceptibility are increased by e.g. the decrease of temperature [33] and the increase of packing fraction [7]. This implies the existence of *dynamic criticality* in thermally/athermally driven disordered systems, i.e. critical slowing down (the divergence of relaxation time τ^*) is accompanied by the divergence of correlation length ξ^*, where the correlation length is roughly estimated as $\xi^* \sim \chi_s^{*1/d}$ in d-dimension [34].

In our MD simulations, however, we find that χ_s^* grows while τ^* shifts to short time scales if the system is dense and sheared quasistatically (Figures 2I,J). This means that instantaneous transverse motions, or "transverse velocities", become more heterogeneous in space than the displacements in long time scales ($\gamma > \gamma_c$). To extract relations between the peak height and position of dynamic susceptibility, we make scatter plots of χ_s^* and $\dot{\gamma}\tau^*$ in Figure 4A. Here, the solid (open) symbols are the results of model A (B), where the shear rate is limited to quasi-static values, $\dot{\gamma}t_0 \leq 10^{-5}$ (10^{-4}). We find that the relations between χ_s^* and $\dot{\gamma}\tau^*$ are well described by the power-laws, where the data of models A and B are fitted to $\dot{\gamma}\tau^* \sim \chi_s^{*-0.82}$ (solid line) and $\chi_s^{*-0.51}$ (dashed line), respectively. The data cannot be described by the power-laws if the shear rate is sufficiently large. Furthermore, the difference between the models becomes significant as χ_s^* decreases and $\dot{\gamma}\tau^*$ increases (Figure 4A), where the two models exhibit different rheological properties, i.e. the Newtonian fluids' behavior and shear thickening, for $\phi < \phi_J$ and $\dot{\gamma}t_0 \ll 1$ (Figure 1). On the other hand, the difference between them is less pronounced if χ_s^* increases and $\dot{\gamma}\tau^*$ decreases (Figure 4A), where both the models show the same rheological behavior, i.e. shear thinning, for $\phi > \phi_J$ and $\dot{\gamma}t_0 \ll 1$ (Figure 1).

3.4 Shear-induced diffusion coefficient

It had been suggested by the elastoplastic model [35] that the diffusion coefficient of sheared athermal system is linked to the peak height of dynamic susceptibility as

$$D \sim \chi_s^* \dot{\gamma} \,. \tag{7}$$

We examine this linear scaling relation between D and $\chi_s^* \dot{\gamma}$ by our numerical data. Extracting the shear-induced diffusion coefficient over the shear rate from the slope of MSD as $D/\dot{\gamma} = \lim_{\tau \to \infty} \Delta^2(\tau)/2\gamma$ [42], we make scatter plots of $D/\dot{\gamma}$ and χ_s^* in Figure 4B. We find that the results of model A (solid symbols) obey the linear scaling, Eq. 7 (solid line), regardless of the packing fraction ϕ, where the shear rate is limited to the quasi-static values, $\dot{\gamma} t_0 \leq 10^{-5}$. However, the model B (open symbols) exhibits a different scaling, $D/\dot{\gamma} \sim \chi_s^{*0.43}$ (dashed line), for any ϕ and $\dot{\gamma} t_0 \leq 10^{-4}$. Though the scaling for the results of model B is controversial, the difference between the models for small χ_s^* can be associated with the different rheological properties in $\phi < \phi_J$ and $\dot{\gamma} t_0 \ll 1$ (Figure 1). In contrast, the difference becomes small if χ_s^* increases, where the same shear thinning, $\eta \sim \dot{\gamma}^{-1}$, is observed in both the models (Figure 1). Interestingly, the product of shear-induced diffusion coefficient D and time scale $\tau^\star$ is almost constant, $D\tau^\star \sim$const., if the maximum intensity increases to $\chi_s^* > 20$ (see SM [41]). This relation, $D\tau^\star \sim$const., is insensitive to the models and mimics the Stokes-Einstein relation [46, 47]. However, the dependence of shear viscosity η on either χ_s^* or $\tau^\star$ is not monotonous (see SM [41]) and we cannot find a clear relationship between the viscosity and diffusion coefficient.

4 Discussion

In this study, we have numerically investigated shear-induced diffusion and dynamic heterogeneities in two-dimensional dense granular flows. Applying simple shear deformations to the system, we analyzed fluctuating transverse motions of the particles, where we focused on the role of packing fraction of the particles ϕ and shear rate $\dot{\gamma}$. To examine the influence of different rheological properties, we introduced two different force laws to the damping force between the particles in contact (as the models A and B). We found that the transverse displacements (Eq. 1) are described as the normal diffusion if the applied strain exceeds the cross-over strain, $\gamma_c < 1$. In long time scales, $\gamma > \gamma_c$, the time correlations of transverse velocities vanish and the transverse displacements obey Gaussian distributions, where most of the transverse displacements exceed the particle radius. In short time scales, $\gamma < \gamma_c$, memory effects on the transverse velocities are strongly suppressed and the transverse displacements become highly non-Gaussian if the system is dense ($\phi > \phi_J$) and sheared quasistatically ($\dot{\gamma} t_0 \ll 1$). We confirmed that the dependence of the MSDs, VACFs, and non-Gaussian parameters on the control parameters, ϕ and $\dot{\gamma}$, is qualitatively the same even if we change the model of contact damping. Different from thermally activated molecular motions in glasses [33], we did not observe any plateaus in the MSDs and self-intermediate scattering functions, and did not find any peaks in the non-Gaussian parameters. Therefore, neither the caging nor sub-diffusion exists in our shear-driven granular systems. In contrast, the dynamic susceptibility exhibits a peak at a characteristic time scale $\tau^\star$. Increasing ϕ and decreasing $\dot{\gamma}$, we found that the maximum of dynamic susceptibility χ_s^* increases though the peak position $\dot{\gamma}\tau^\star$ shifts to short time scales. This trend is opposite to the dynamic criticality observed in glasses [48] and homogeneously driven granular materials [7], where we described our numerical results in a quasi-static regime as a power-law, $\dot{\gamma}\tau^\star \sim \chi_s^{*-\nu}$, with the model-dependent exponent ν. Moreover, the diffusion coefficient over the shear rate, $D/\dot{\gamma}$, is linear in the maximum of dynamic susceptibility χ_s^* (Eq. 7) if the model A is used for the contact damping. On the other hand, we found a sub-linear scaling between them, which is in conflict to the prediction made by the elastoplastic model [35], if the model B is used in MD simulations.

Though we have examined two different models of contact damping, where they exhibit the Newtonian fluids' behavior and Bagnold scaling for sufficiently small ϕ and $\dot{\gamma}$ [38], more systematic studies of the damping force are also possible [38, 49]. Furthermore, the effect of particle inertia which we have not studied here is also crucial to the rheology [50]. In general, interactions between the particles in contact drastically change the rheological behavior, e.g. frictional contacts induce *discontinuous shear thickening* [51, 52], whereas cohesive contacts result in *discontinuous shear thinning* [53]. Because our results suggest that the relation between the maximum intensity and characteristic time scale for dynamic heterogeneities, as well as the link between the shear-induced diffusion and dynamic heterogeneities, is dependent on rheological properties, further studies of the effect of particle inertia and interaction forces are necessary in future. In addition, different models of elastic forces, e.g. the Hertzian contact which takes account of the particle curvature, should also be examined. Moreover, non-spherical particle shapes [54] and the study in three dimensions [55, 56] are also important for experiments and industrial applications of this study.

5 Conclusion

In conclusion, we found that shear-induced transverse motions of granular particles are totally different from thermally activated molecular motions in glasses. The scaling relations between the maximum intensity of dynamic

heterogeneities, characteristic time scale, and diffusion coefficient of the particles were confirmed in quasi-static flows, where the scaling exponents are dependent on the model of contact damping.

Data availability statement

The raw data supporting the conclusion of this article will be made available by the authors, without undue reservation.

Author contributions

KS and TK designed the research and wrote the article. KS performed the research.

Funding

This work was supported by KAKENHI Grant Nos. 20H01868, 21H01006, 22K03459, JPMJFR212T, 20H05157, 20H00128, 19K03767, 18H01188 from JSPS.

Conflict of interest

The authors declare that the research was conducted in the absence of any commercial or financial relationships that could be construed as a potential conflict of interest.

Publisher's note

All claims expressed in this article are solely those of the authors and do not necessarily represent those of their affiliated organizations, or those of the publisher, the editors and the reviewers. Any product that may be evaluated in this article, or claim that may be made by its manufacturer, is not guaranteed or endorsed by the publisher.

Supplementary material

The Supplementary Material for this article can be found online at: https://www.frontiersin.org/articles/10.3389/fphy.2022.992239/full#supplementary-material

References

1. Jeager H, Nagel S, Behringer R. Granular solids, liquids, and gases. *Rev Mod Phys* (1996) 68:1259. doi:10.1103/RevModPhys.68.1259

2. Bonn D, Denn MM, Berthier L, Divoux T, Manneville S. Yield stress materials in soft condensed matter. *Rev Mod Phys* (2017) 89:035005. doi:10.1103/revmodphys.89.035005

3. Aranson IS, Tsimring LS. Patterns and collective behavior in granular media: Theoretical concepts. *Rev Mod Phys* (2006) 78:641–92. doi:10.1103/revmodphys.78.641

4. Castellanos A. The relationship between attractive interparticle forces and bulk behaviour in dry and uncharged fine powders. *Adv Phys X* (2005) 54:263–376. doi:10.1080/17461390500402657

5. Pouliquen O. Velocity correlations in dense granular flows. *Phys Rev Lett* (2004) 93:248001. doi:10.1103/physrevlett.93.248001

6. Dauchot O, Marty G, Biroli G. Dynamical heterogeneity close to the jamming transition in a sheared granular material. *Phys Rev Lett* (2005) 95:265701. doi:10.1103/physrevlett.95.265701

7. Keys AS, Abate AR, Glotzer SC, Durian DJ. Measurement of growing dynamical length scales and prediction of the jamming transition in a granular material. *Nat Phys* (2007) 3:260–4. doi:10.1038/nphys572

8. Candelier R, Dauchot O, Biroli G. Building blocks of dynamical heterogeneities in dense granular media. *Phys Rev Lett* (2009) 102:088001. doi:10.1103/physrevlett.102.088001

9. Katsuragi H, Abate AR, Durian DJ. Jamming and growth of dynamical heterogeneities versus depth for granular heap flow. *Soft Matter* (2010) 6:3023. doi:10.1039/b918991b

10. Nordstrom KN, Gollub JP, Durian DJ. Dynamical heterogeneity in soft-particle suspensions under shear. *Phys Rev E* (2011) 84:021403. doi:10.1103/physreve.84.021403

11. Rahmani Y, van der Vaart K, van Dam B, Hu Z, Chikkadi V, Schall P. Dynamic heterogeneity in hard and soft sphere colloidal glasses. *Soft Matter* (2012) 8:4264. doi:10.1039/c2sm25267h

12. Sanlí C, Saitoh K, Luding S, van der Meer D. Collective motion of macroscopic spheres floating on capillary ripples: Dynamic heterogeneity and dynamic criticality. *Phys Rev E* (2014) 90:033018. doi:10.1103/physreve.90.033018

13. Heussinger C, Barrat JL. Jamming transition as probed by quasistatic shear flow. *Phys Rev Lett* (2009) 102:218303. doi:10.1103/physrevlett.102.218303

14. Vågberg D, Olsson P, Teitel S. Universality of jamming criticality in overdamped shear-driven frictionless disks. *Phys Rev Lett* (2014) 113:148002. doi:10.1103/physrevlett.113.148002

15. Tsamados M. Plasticity and dynamical heterogeneity in driven glassy materials. *Eur Phys J E* (2010) 32:165–81. doi:10.1140/epje/i2010-10609-0

16. Hatano T. Rheology and dynamical heterogeneity in frictionless beads at jamming density. *J Phys : Conf Ser* (2011) 319:012011. doi:10.1088/1742-6596/319/1/012011

17. Heussinger C, Berthier L, Barrat JL. Superdiffusive, heterogeneous, and collective particle motion near the fluid-solid transition in athermal disordered materials. *Eur Phys Lett* (2010) 90:20005. doi:10.1209/0295-5075/90/20005

18. Goldenberg C, Tanguy A, Barrat JL. Particle displacements in the elastic deformation of amorphous materials: Local fluctuations *vs.* non-affine field. *Europhys Lett* (2007) 80:16003. doi:10.1209/0295-5075/80/16003

19. Saitoh K, Mizuno H. Anomalous energy cascades in dense granular materials yielding under simple shear deformations. *Soft Matter* (2016) 12:1360–7. doi:10.1039/c5sm02760h

20. Olsson P, Teitel S. Critical scaling of shear viscosity at the jamming transition. *Phys Rev Lett* (2007) 99:178001. doi:10.1103/physrevlett.99.178001

21. Geng J, Behringer RP. Diffusion and mobility in a stirred dense granular material. *Phys Rev Lett* (2004) 93:238002. doi:10.1103/physrevlett.93.238002

22. Eisenmann C, Kim C, Mattsson J, Weitz DA. Shear melting of a colloidal glass. *Phys Rev Lett* (2010) 104:035502. doi:10.1103/physrevlett.104.035502

23. Wandersman E, Dijksman JA, van Hecke M. Particle diffusion in slow granular bulk flows. *Eur Phys Lett* (2012) 100:38006. doi:10.1209/0295-5075/100/38006

24. Besseling R, Weeks ER, Schofield AB, Poon WCK. Three-dimensional imaging of colloidal glasses under steady shear. *Phys Rev Lett* (2007) 99:028301. doi:10.1103/physrevlett.99.028301

25. Möbius ME, Katgert G, van Hecke M. Relaxation and flow in linearly sheared two-dimensional foams. *Eur Phys Lett* (2010) 90:44003. doi:10.1209/0295-5075/90/44003

26. Ono IK, Tewari S, Langer SA, Liu AJ. Velocity fluctuations in a steadily sheared model foam. *Phys Rev E* (2003) 67:061503. doi:10.1103/physreve.67.061503

27. Olsson P. Diffusion and velocity autocorrelation at the jamming transition. *Phys Rev E* (2010) 81:040301(R). doi:10.1103/physreve.81.040301

28. Kharel P, Rognon P. Vortices enhance diffusion in dense granular flows. *Phys Rev Lett* (2017) 119:178001. doi:10.1103/physrevlett.119.178001

29. Lemaitre A, Caroli C. Rate-dependent avalanche size in athermally sheared amorphous solids. *Phys Rev Lett* (2009) 103:065501. doi:10.1103/physrevlett.103.065501

30. Clemmer JT, Salerno KM, Robbins MO. Criticality in sheared, disordered solids. II. Correlations in avalanche dynamics. *Phys Rev E* (2021) 103:042606. doi:10.1103/physreve.103.042606

31. Cai R, Xiao H, Zheng J, Zhao Y. Diffusion of size bidisperse spheres in dense granular shear flow. *Phys Rev E* (2019) 99:032902. doi:10.1103/physreve.99.032902

32. Heussinger C, Barrat JL. Jamming transition as probed by quasistatic shear flow. *Phys Rev Lett* (2009) 102:218303. doi:10.1103/physrevlett.102.218303

33. Berthier L, Biroli G. Theoretical perspective on the glass transition and amorphous materials. *Rev Mod Phys* (2011) 83:587–645. doi:10.1103/revmodphys.83.587

34. Berthier L. Dynamic heterogeneity in amorphous materials. *Physics* (2011) 4:42. doi:10.1103/physics.4.42

35. Martens K, Bocquet L, Barrat JL. Connecting diffusion and dynamical heterogeneities in actively deformed amorphous systems. *Phys Rev Lett* (2011) 106:156001. doi:10.1103/physrevlett.106.156001

36. Lechenault F, Dauchot O, Biroli G, Bouchaud JP. Lower bound on the four-point dynamical susceptibility: Direct experimental test on a granular packing. *Europhys Lett* (2008) 83:46002. doi:10.1209/0295-5075/83/46002

37. Saitoh K, Hatano T, Ikeda A, Tighe BP. Stress relaxation above and below the jamming transition. *Phys Rev Lett* (2020) 124:118001. doi:10.1103/physrevlett.124.118001

38. Vågberg D, Olsson P, Teitel S. Dissipation and rheology of sheared soft-core frictionless disks below jamming. *Phys Rev Lett* (2014) 112:208303. doi:10.1103/physrevlett.112.208303

39. Luding S. Anisotropy in cohesive, frictional granular media. *J Phys : Condens Matter* (2005) 17:S2623–40. doi:10.1088/0953-8984/17/24/017

40. In our MD simulations, numerical values of k_e and η_d are given by 1.0 and 0.1, respectively.

41. See Supplemental Material at [URL will be inserted by publisher] for full details.

42. Saitoh K, Kawasaki T. Critical scaling of diffusion coefficients and size of rigid clusters of soft athermal particles under shear. *Front Phys* (2020) 8:99. doi:10.3389/fphy.2020.00099

43. Boon JP, Yip S. *Molecular hydrodynamics*. New York: Dover (1991).

44. Saitoh K, Mizuno H. Anisotropic decay of the energy spectrum in two-dimensional dense granular flows. *Phys Rev E* (2017) 96:012903. doi:10.1103/physreve.96.012903

45. Chaudhuri P, Berthier L, Kob W. Universal nature of particle displacements close to glass and jamming transitions. *Phys Rev Lett* (2007) 99:060604. doi:10.1103/physrevlett.99.060604

46. Kawasaki T, Onuki A. Slow relaxations and stringlike jump motions in fragile glass-forming liquids: Breakdown of the Stokes-Einstein relation. *Phys Rev E* (2013) 87:012312. doi:10.1103/physreve.87.012312

47. Kawasaki T, Kim K. Identifying time scales for violation/preservation of Stokes-Einstein relation in supercooled water. *Sci Adv* (2017) 3:e1700399. doi:10.1126/sciadv.1700399

48. Lačević N, Starr FW, Schrøder TB, Glotzer SC. Spatially heterogeneous dynamics investigated via a time-dependent four-point density correlation function. *J Chem Phys* (2003) 119:7372–87. doi:10.1063/1.1605094

49. Andreotti B, Barrat JL, Heussinger C. Shear flow of non-brownian suspensions close to jamming. *Phys Rev Lett* (2012) 109:105901. doi:10.1103/physrevlett.109.105901

50. Kawasaki T, Ikeda A, Berthier L. Thinning or thickening? Multiple rheological regimes in dense suspensions of soft particles. *Eur Phys Lett* (2014) 107:28009. doi:10.1209/0295-5075/107/28009

51. Otsuki M, Hayakawa H. Critical scaling near jamming transition for frictional granular particles. *Phys Rev E* (2011) 83:051301. doi:10.1103/physreve.83.051301

52. Seto R, Mari R, Morris JF, Denn MM. Discontinuous shear thickening of frictional hard-sphere suspensions. *Phys Rev Lett* (2013) 111:218301. doi:10.1103/physrevlett.111.218301

53. Irani E, Chaudhuri P, Heussinger C. Impact of attractive interactions on the rheology of dense athermal particles. *Phys Rev Lett* (2014) 112:188303. doi:10.1103/physrevlett.112.188303

54. Marschall T, Keta YE, Olsson P, Teitel S. Orientational ordering in athermally sheared, aspherical, frictionless particles. *Phys Rev Lett* (2019) 122:188002. doi:10.1103/physrevlett.122.188002

55. Oyama N, Mizuno H, Saitoh K. Avalanche interpretation of the power-law energy spectrum in three-dimensional dense granular flow. *Phys Rev Lett* (2019) 122:188004. doi:10.1103/physrevlett.122.188004

56. Olsson P. Dimensionality and viscosity exponent in shear-driven jamming. *Phys Rev Lett* (2019) 122:108003. doi:10.1103/physrevlett.122.108003